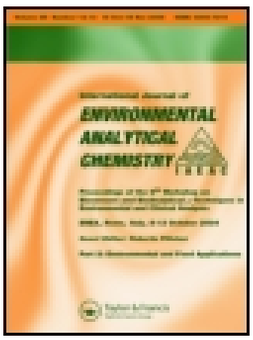

International Journal of Environmental Analytical Chemistry

ISSN: (Print) (Online) Journal homepage: https://www.tandfonline.com/loi/geac20

A simple spectrophotometric study of adsorption of Hg(II) on glycine functionalised magnetic nanoparticle entrapped alginate beads

Surbhi Lilhare, Sunitha B. Mathew, Ajaya Kumar Singh & Sreevidya Sankarasubramanian

To cite this article: Surbhi Lilhare, Sunitha B. Mathew, Ajaya Kumar Singh & Sreevidya Sankarasubramanian (2021): A simple spectrophotometric study of adsorption of Hg(II) on glycine functionalised magnetic nanoparticle entrapped alginate beads, International Journal of Environmental Analytical Chemistry, DOI: 10.1080/03067319.2021.1884242

To link to this article: https://doi.org/10.1080/03067319.2021.1884242

Published online: 01 Mar 2021.

INTERNATIONAL JOURNAL OF ENVIRONMENTAL ANALYTICAL CHEMISTRY
https://doi.org/10.1080/03067319.2021.1884242

Taylor & Francis
Taylor & Francis Group

A simple spectrophotometric study of adsorption of Hg(II) on glycine functionalised magnetic nanoparticle entrapped alginate beads

Surbhi Lilhare[a], Sunitha B. Mathew[a], Ajaya Kumar Singh[a] and Sreevidya Sankarasubramanian[b]

[a]Department of Chemistry, Govt. V. Y. T. Postgraduate Autonomous College, Durg, India; [b]Department of Chemistry, Kalyan P.G. College, Durg, India

ABSTRACT

In this study, a simple spectrophotometric method has been applied to investigate the adsorption of Hg(II) from aqueous solution on glycine functionalised magnetic nanoparticles entrapped calcium alginate beads (GFMNPECABs) from aqueous solution. The adsorbent was characterised by Fourier Transform Infrared (FT-IR) spectroscopy, Scanning Electron Microscopy (SEM), X-ray Diffraction (XRD) and Brunauer-Emmett-Teller (BET) analysis. The influence of pH, contact time, temperature, adsorbent dose etc. were studied and optimised. The results of batch adsorption experiment showed that maximum adsorption capacity of 3.59 mg g^{-1} was obtained at pH 5 and 65 minutes of contact time.The adsorption behaviour of Hg(II) was evaluated using Langmuir, Freundlich and Temkin isotherm and it was found that the data best fitted with the Freundlich model. The kinetic study revealed that the adsorption follows pseudo-second-order kinetics with a high correlation coefficient of $R^2 = 0.9998$. The thermodynamic investigation verified the endothermic and spontaneous nature of the adsorption process with an enthalpy change (ΔH) and entropy change (ΔS) of 20.25 kJ mol^{-1} and 79.88 J mol^{-1} K, respectively. The adsorption studies were monitored based on the reaction of Hg(II) with iodine and leucocrystal violet. This study shows that GFMNPECABs is a promising adsorbent for removal of Hg(II) from aqueous solution and the above spectrophotometric method could be satisfactorily applied for adsorption studies.

ARTICLE HISTORY
Received 6 October 2020
Accepted 14 January 2021

KEYWORDS
Mercury; adsorption; magnetic nanoparticles; glycine functionalised; calcium alginate; spectrophotometric method

1. Introduction

Mercury(II) (Hg^{2+}) is one of the most dangerous pollutants because of its toxic or carcinogenic properties. It's occurrence is rare in the Earth's crust (0.1–1.0 mg L^{-1}) [1]. Some inorganic and organic mercury compounds are extremely toxic and cause serious threat to human beings and to natural environment. The maximum acceptable content of Hg(II) for human beings as recommended by World Health Organization (WHO) in drinking water is 1 µg L^{-1} [2]. Hg(II) finds its wide applications in industries, that produce electrical equipment, paints, pesticides, pulp and paper, domestic thermometers, and medicines. The main sources of Hg(II) emission to land, water, and air are by the process of mining of

CONTACT Ajaya Kumar Singh ajayaksingh_au@yahoo.co.in

ore and smelting (in particular Cu and Zn smelting), burning of fossil fuels (mainly coal), industrial production processes, and consumption related discharges (including waste incineration) [3]. The waste water discharged from electroplating, metal finishing operations, electronic-circuit production, steel and nonferrous processes, chemical, pharmaceutical production industries, chlor-alkali, fertiliser, pulp and paper, plastic, battery manufacturing, oil refining, paints and electrical components are the major sources of Hg(II) in the environment [4–6]. Thus, Hg(II) is very useful indispensable metal for industries on one hand and one of the typical environmental pollutants on the other hand. Controlling the concentration of heavy metals in waste, before it is discharged, is very important. Therefore, it is very important to develop techniques to recover Hg(II) from various kinds of waste water containing Hg(II).

Various techniques are available to treat wastewater such as chemical precipitation [7], coagulation [8], reverse osmosis [9], precipitation [10], membrane separation [11] and ion-exchange [12]. Electro deposition, biological treatment, solid phase extraction and adsorption are among the most common methods for the elimination of heavy metals [13–16], but most of them suffer from various disadvantages such as high expense, prolonged process with less efficiency, production of other waste products, etc. Among these techniques, adsorption method is the most simple and effective technique to remove Hg(II) from waste water [17,18]. Adsorption is considered as the most promising technique due to its simplicity of design, ease of operation, selectivity, high efficiency, low cost, and operational convenience [19–24].

Alginate is widely used as an effective adsorbent, which is non-toxic, biodegradable and inexpensive [25,26]. Pure magnetic nanoparticles (MNPs) are not applied directly in adsorption process due to their strong dipole-dipole attraction that might cause aggregation. Therefore, magnetic nanoparticles are entrapped into various types of organic and inorganic stabilisers such as activated carbon [27], chitosan [27–31], alginate biopolymer [32–34] and β-cyclodextrin [35,36]. Adsorption studies of Hg(II) have been reported using UV-Visible spectrophotometer, AAS etc [37,38]. Here the chromogenic system consisting of iodine and leucocrystal violet (LCV) has been used for the study of adsorption.

In our present work, adsorption of Hg(II) with glycine functionalised magnetic nanoparticle entrapped in calcium alginate beads using a simple spectrophotometric method has been proposed. The various parameters like adsorption capacity, separation and recovery processes were studied. GFMNPECABs has been reported as an effective adsorbent for the removal of metals like Cu(II) [39] due to their large surface area and presence of amino groups on the surface after functionalization. The performance and efficiency of GFMNPECABs as adsorbent for removal of Hg(II) has been evaluated and influence of variables like time, temperature, pH was investigated by batch method. Analysis of adsorption isotherm models were made and the reusability was checked to explore the possibility of removal of Hg(II) ions from effluents using this adsorbent.

2. Materials and methods

2.1. Materials

All chemicals used were of analytical grade and used without further purification. All solutions were prepared in double-distilled water. Glycine ($C_2H_5NO_2$), iodine (I_2) and 85% phosphoric

acid were purchased from Merck (Mumbai) India. Mercuric chloride ($HgCl_2$), calcium chloride ($CaCl_2$), NaOH and HCl were obtained from Loba Chemical Pvt Ltd (Mumbai) India. Sodium alginate ($C_6H_9NaO_7$) was received from Sigma-Aldrich (USA). Ferric chloride hexahydrate ($FeCl_3.6H_2O$), ferrous chloride dihydrate ($FeCl_2.2H_2O$) and NH_4OH from CDH, and LCV from HiMedia Laboratories (Mumbai) India were purchased.

2.2. Equipment

X-Ray diffraction (XRD) (Expert-Pro PW3064/60) analysis was done at 30° to 80°. Fourier transform-infrared (FT-IR) spectrometer (Thermo Nicolet Avtar 370) was used to record the infrared spectra in the range of 1000–4000 cm^{-1} using KBr pellets and the Scanning Electron Microscopic (SEM) (Jeol 6390LA/OXFORD XMX N) images of GFMNPECABs before and after adsorption were obtained. N_2 gas adsorption–desorption studies of GFMNPECABs were done by Brunauer-Emmett-Teller (BET) analysis at constant temperature. A Systronics UV-visible spectrophotometer-117 (Carry 50 scan, Varian) with 1 cm quartz cell (1.0 ml) was used for the measurement of absorbance. The pH measurement was carried out using a digital pH metre (Systronics model-112). The temperature was kept constant with the help of the thermostatic water bath.

2.3. Synthesis of glycine functionalised magnetic nanoparticles (GFMNPs)

Under hydrothermal condition, iron nanoparticles (NPs) were synthesised by co-precipitation method [40]. Fe(II) salt and Fe(III) salt in the molar ratio 2:1 were mixed and dissolved in double-distilled water. To this, 1.5 M NH_4OH solution was added dropwise at 25–30°C under vigorous stirring. It resulted in the formation of a black precipitate of iron nanoparticles which were magnetically separated and washed. The black wet precipitate was then transferred to a 250 ml Erlenmeyer flask and10 ml of 0.1% glycine in double distilled water was added dropwise leading to wet functionalization. The content formed was kept at 80°C for 30 minutes. The synthesised glycine functionalised Fe_3O_4 NPs were isolated using external magnetic field, washed several times with double distilled water and dried in an oven at 200°C for 2 hours.

2.4. Preparation of glycine functionalised magnetic nanoparticles entrapped calcium alginate beads (GFMNPECABs)

GFMNPECABs were prepared following the trends of Verma et al. with few modifications [39]. Here in our work, we had used the wet functionalization with glycine onto the wet magnetic nanoparticles and its subsequent entrapment into alginate to get potential beads. The beads were then washed several times with double distilled water and stored in double-distilled water for later use as an adsorbent. The beads turned reddish brown as a result of entrapment of modified magnetic NPs by the alginate polymer. A representative photograph of gel beads (GFMNPECABs), is shown in Figure 1.

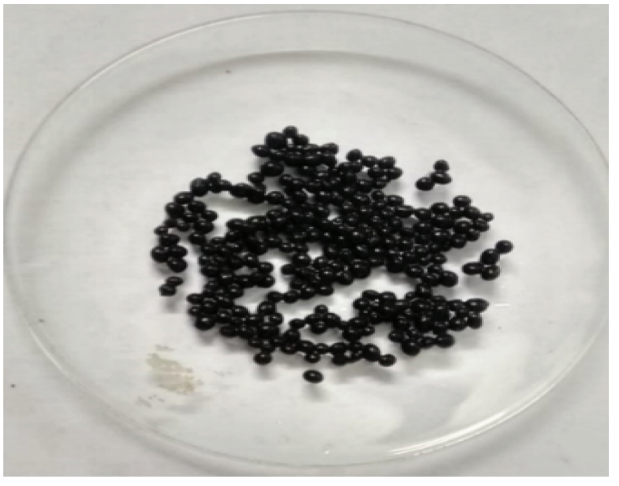

Figure 1. Photograph of GFMNPECABs.

2.5. Procedure for Hg(II) analysis

After adsorption procedure, the beads and liquid phases were separated by normal filter paper and the mercury (II) concentration of the filtrate was determined spectrophotometrically using iodine (I_2) and LCV. To 5 ml of the filtrate, 0.2 ml iodine (0.004 g of solid iodine in 0.8 ml of acetic acid and diluting with distilled water to 20 ml) and 2 ml LCV (0.025 g in 20 ml double distilled water containing 0.3 ml of phosphoric acid) were added which gave violet coloured dye of crystal violet (CV). The absorbance was measured at 590 nm [41].

2.6. Batch adsorption experiment

The percentage removal (R%) of Hg(II) ions by GFMNPECABs was studied by batch adsorption experiment. The experiments were carried out by varying the pH ranging from 3.0 to 8.0, contact time, 5–80 min; adsorbent dose, 0.1–1.0 g ml^{-1}; and concentration of Hg(II) solution; 5–30 mg L^{-1}. An aqueous solution of 0.1 M HCl/0.1 M NaOH was used for pH value adjustment. In a typical experiment 10 ml of 10 mg L^{-1} Hg(II) was shaken with 0.8 g of GFMNPECABs with a speed of 150 rpm at a pH of 5.0 and 30°C for 65 min. After adsorption, the adsorbents were separated by filter paper and then concentration of the Hg^{2+} solutions was determined using a simple spectrophotometric method as mentioned under analysis procedure.The beads were characterised using XRD, FT-IR, SEM and BET before and after adsorption. The percentage removal of Hg(II) ions is calculated using Equation (1).

$$R\% = \frac{C_0 - C_e}{C_0} \times 100 \tag{1}$$

The amount of Hg(II) ion adsorbed (q_e) was calculated using this equation:

$$q_e = \frac{(C_0 - C_e)V}{m} \tag{2}$$

where C_0 and C_e are the initial and equilibrium concentrations of Hg(II) ions (mg L^{-1}), respectively, m is the mass of adsorbent (g) and V is the volume of the solution (L) [42].

3. Results and discussion

3.1. Characterisation of adsorbent

3.1.1. X-Ray diffraction (XRD) analysis

The XRD patterns of GFMNPECABs before and after adsorption exhibit six similar characteristic peaks as shown in Figure 2. The positions of the peaks correspond to 2θ = 30.30°, 35.68°, 43.20°, 53.74°, 57.44° and 62.94° with indices of (2 2 0), (3 1 1), (4 0 0), (4 2 2), (5 1 1) and (4 4 0) for the two samples. The intensity of the diffraction peak indicates that GFMNPECABs has aspinel structure. The samples show sharp peaks, indicating the ultrafine nature and small crystallite size of the particles and these results matched with the planes of cubic cell (face-centred cubic) structure. The average crystal size (D) of GFMNPECABs before and after adsorption was determined by Debye-Scherrer's equation [43]:

$$D = \frac{K.\lambda}{\beta.\cos\theta} \tag{3}$$

where D is average crystal size in Å, θ is the peak angle, β is FWHM (Full Width at Half Maximum) of the peak, λ is the wavelength of X-ray and K is constant (K = 0.9). In this case, the calculated average crystal size of GFMNPECABs before and after adsorption were 2.8875 and 8.011 nm.

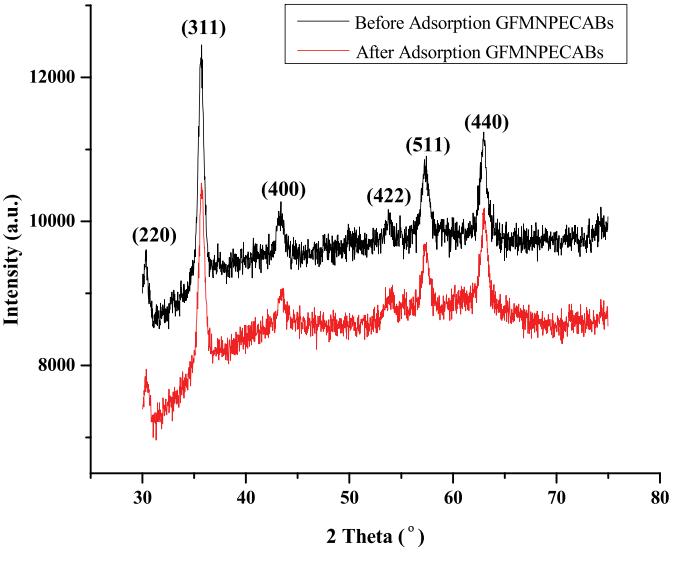

Figure 2. XRD patterns of GFMNPECABs before and after adsorption.

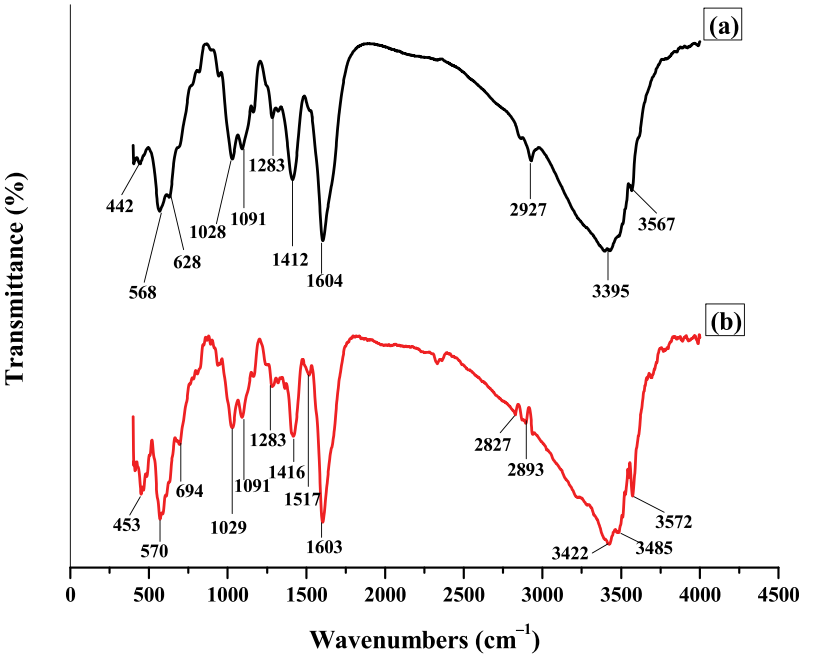

Figure 3. The FT-IR spectra of GFMNPECABs before (a) and after (b) adsorption of Hg(II).

3.1.2. Fourier transform infrared (FT-IR) spectroscopy studies

The various bands of FT-IR spectra for GFMNPECABs before and after adsorption is shown in Figure 3, which indicates the presence of several functional groups involved in the process. The bands at 568 cm^{-1} and 570 cm^{-1} is due to Fe–O stretching vibration before and after adsorption. This result is found to be consistent with the literature [44–46]. The strong broad absorption band and weak bands around 3300–3600 cm^{-1} is associated with stretching vibrations of O–H bond and NH stretching vibrations. Stretching vibration bands of C–H are observed in the region 2800–2950 cm^{-1} [47,48]. The vibrational modes in the region 1400–1600 cm^{-1} may be attributed to the stretching and deformation absorption bands of COO^- and NH_3 groups [49]. The sharp bands at 1412, 1604 cm^{-1} and 1416, 1603 cm^{-1} correspond to symmetric and asymmetric stretching vibrations of COO^- group of glycine and alginate [50]. The shift in the band from 3393 cm^{-1} and 3567 cm^{-1} to 3422 cm^{-1} and 3572 cm^{-1} with an additional small peak at 3485 cm^{-1} after adsorption indicates the electrostatic interaction of OH and NH group with Hg(II) [47,51]. The variation in intensity of band 1400 cm^{-1} and 1600 cm^{-1} with a small additional peak at 1517 cm^{-1} after adsorption indicates involvement of COO^- and NH_3 group in the adsorption process.

3.1.3. Scanning electron microscopic (SEM) analysis

The scanning electron microscopic (SEM) analysis images of GFMNPECABs before and after adsorption (Figure 4), indicate that the surface of GFMNPECABs was rough with a large surface area. The surface morphology of GFMNPECABs before adsorption of Hg(II) indicated an irregular structure with large surface area as compared to that of after adsorption showing the availability of the free sites on the adsorbent for adsorption.

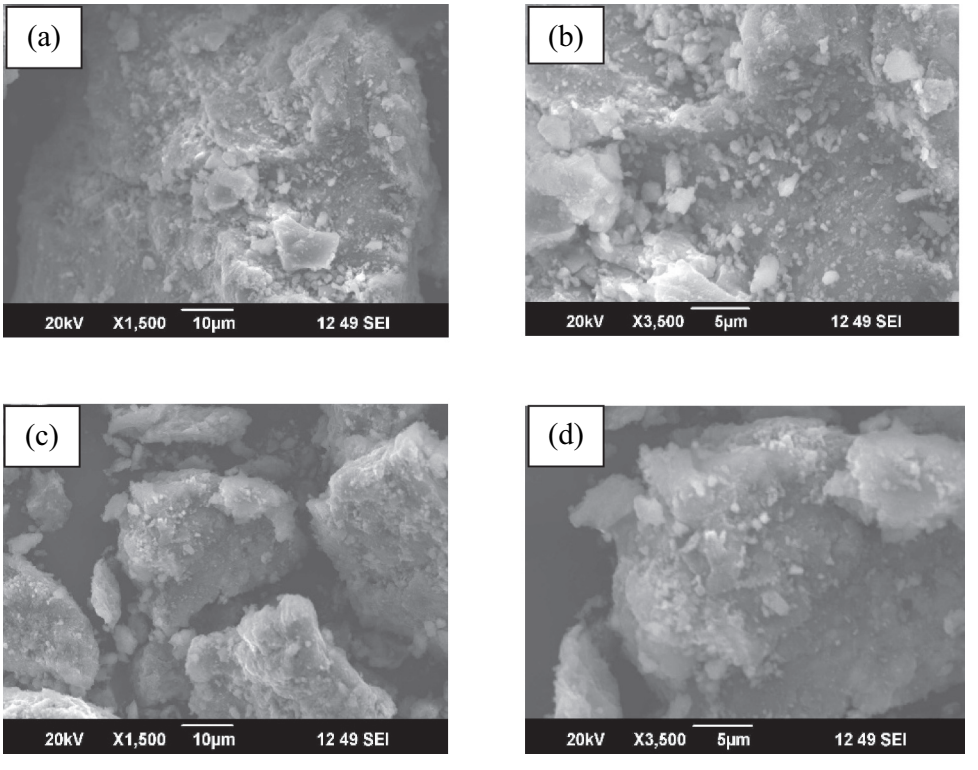

Figure 4. SEM images of GFMNPECABs before (a,b) and after (c,d) adsorption of Hg(II) at different magnification.

3.1.4. Brunauer-Emmett-Teller (BET) analysis

Brunauer-Emmett-Teller (BET) method was applied for the determination of surface area of the adsorbent. Figure 5 shows the N_2 adsorption and desorption isotherm behaviour for GFMNPECABs at 77.35 K. All isotherms exhibit Type IV profile according to the IUPAC classification [52], with hysteresis loop at lower pressure 0.2. This implies that the pores of GFMNPECABs are mostly microporous, mesoporous and macroporous. As seen in figure, almost no nitrogen is adsorbed by GFMNPECABs at very lower relative pressure (P/P_0), indicating that there are micropores in GFMNPECABs. Furthermore, the figure in inset, shows BJH desorption pore size distributions of GFMNPECABs. It could be noted that the pores between 2 and 85 nm were dominant; that is, micropores, mesopores and macropores are present in GFMNPECABs. The BET analysis gave the following results: BET adsorption/desorption surface areas of 15.375 $m^2\ g^{-1}$/32.204 $m^2\ g^{-1}$, BJH adsorption/desorption volumes of pores 0.028 $cm^3\ g^{-1}$/0.029 $cm^3\ g^{-1}$ and pore diameter of 1.085 nm/1.919 nm.

3.2. Effect of pH

The effect of pH on adsorption is an important factor for determining the optimum sorption of Hg(II) ions. The pH was adjusted using different amounts of 0.1 M NaOH or

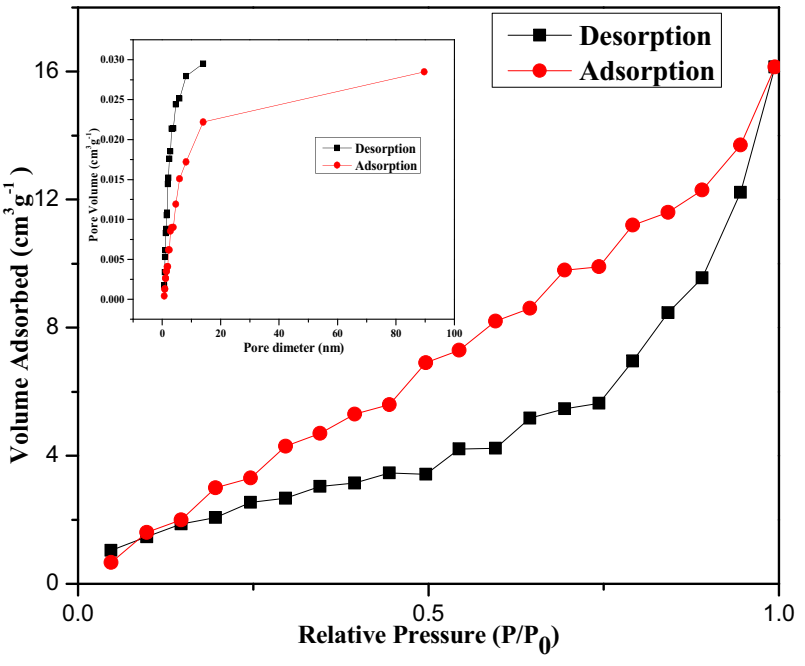

Figure 5. N_2 adsorption-desorption isotherm.

0.1 M HCl. The influence of pH on the adsorption of Hg(II) ions was investigated by varying the pH ranging from 3 to 8 under the following conditions: 10 mg L^{-1} initial Hg(II) concentration, 0.8 g dosage and 30°C temperature and the result is shown in Figure 6. As pH increases, the adsorption capacity of GFMNPECABs increases till pH 5. At pH 5, amino groups are un-protonated, hence, easily donates its lone pair of electron to Hg(II) ion to form complexes on the surface of the adsorbent and thus showed highest adsorption [53]. Increase in pH higher than 5, resulted in decrease in efficiency as the metal ions gets precipitated as insoluble hydroxides. This reduced the concentration of free metal ions and thus decreased the removal capacity. At lower pH, the amino group on the GFMNPECABs could be protonated thereby inducing electrostatic repulsion with the positively charged Hg(II) ions in solution. In addition, the competition between H^+ and Hg(II) ions also could cause low adsorption.

The pH_{pzc} (point of zero charge) for GFMNPECABs value was found to be 4.76 (Figure 7). GFMNPECABs surface was positively charged when pH <pH_{pzc}, and negatively charged at pH > pH_{pzc} [54]. Mercury(II) ion at pH 5 gave maximum adsorption which is above the point of zero charge (pH_{pzc}). The electrostatic attraction and the coordination with the functional groups on GFMNPECABs constitute the primary adsorption mechanism.

3.3. Effect of adsorbent dose

The effect of adsorbent dosage on the percentage removal and adsorbed amount (q_e) was investigated by varying the dose from 0.1 to 1.0 g at pH 5 and the result is shown in

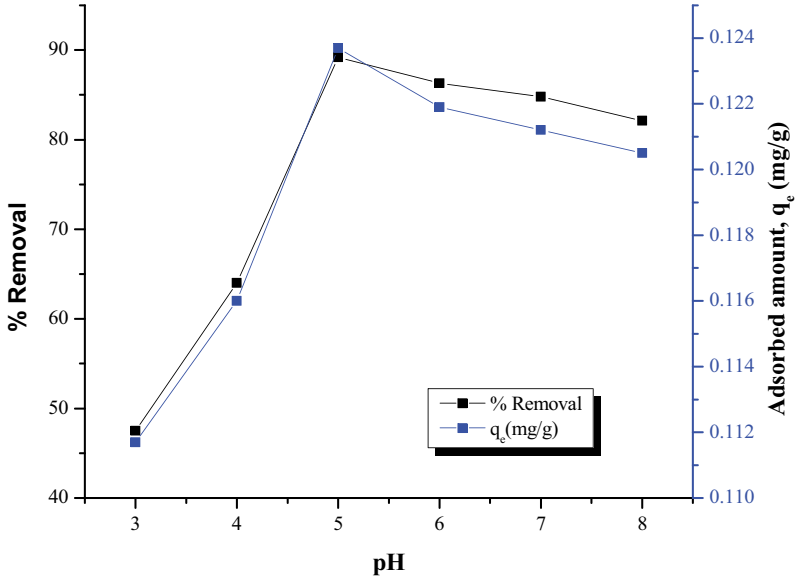

Figure 6. Effect of initial pH on % removal and adsorbed amount of Hg(II) by GFMNPECABs. [Hg(II) = 10 mg L^{-1}, Adsorbent dose = 0.8 g, Time = 65 min and Temperature = 30°C].

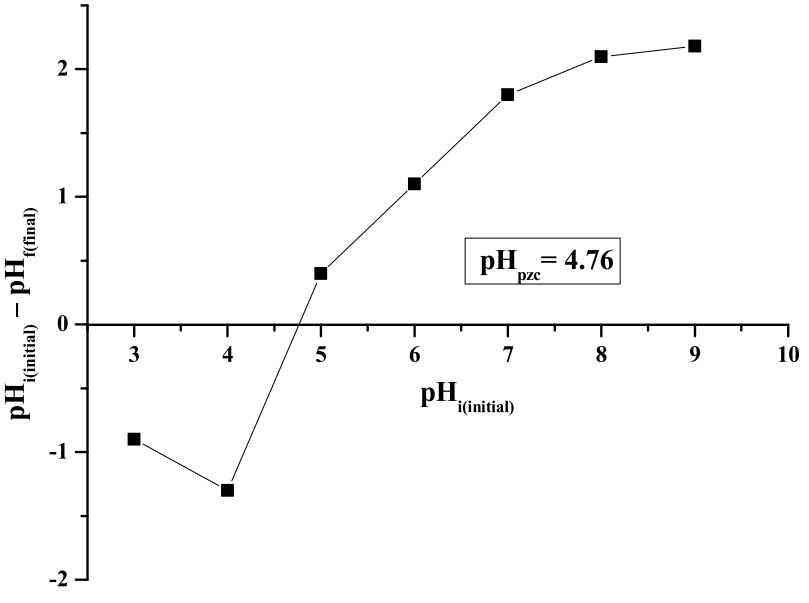

Figure 7. pH_{pzc} (point of zero charge) of GFMNPECABs. [Hg(II) = 10 mg L^{-1}, Adsorbent dose = 0.8 g, Time = 65 min and Temperature = 30°C].

Figure 8. An increment in sorbent dosage causes an increase in the ratio of sorbent weight per solution volume, so the percentage of removal increases. The percent removal is higher due to the increased mass of the solid phase. The percent removal (%) was not affected by increasing the adsorbent dosage over 0.8 g. On increasing adsorbent dose the

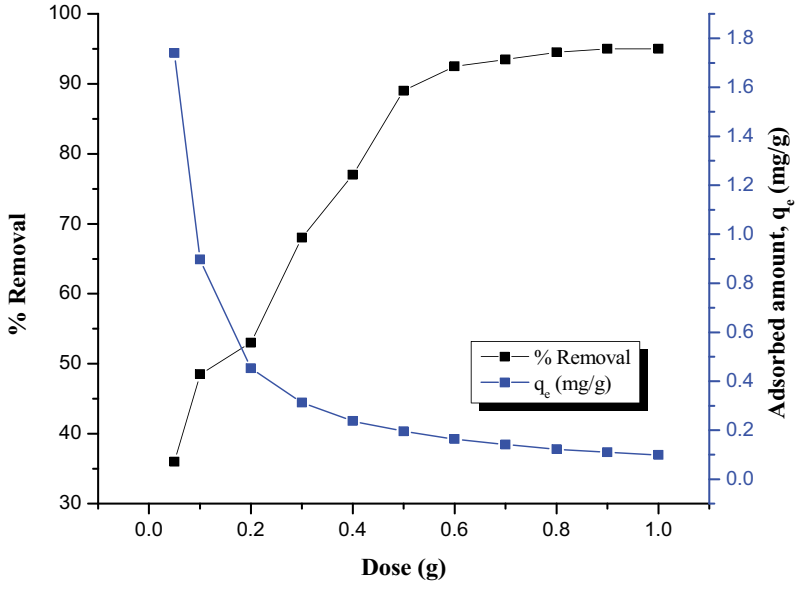

Figure 8. Effect of adsorbent doses on % removal and adsorbed amount of Hg(II). [Hg(II) = 10 mg L^{-1}, Time = 65 min, Temperature = 30°C and pH = 5].

amount of Hg(II) adsorbed per unit mass decreases as the amount of Hg(II) in solution is constant.

3.4. Effect of time

The effect of time on the adsorption of Hg(II) ions by GFMNPECABs was studied up to 80 minutes and the result is shown in Figure 9. A 10 ml solution on of Hg(II) (10 mg L^{-1}) was taken at 5 pH and 0.8 g of adsorbent was added. The content was then shaken at 30°C and analysed at different times. Initially, the uptake of Hg(II) ions by the adsorbent was high and later slowed down after, around 65 min and successively equilibrium was achieved. Adsorption of Hg(II) ions initially increased due to rapid binding at the active sites of adsorbent in a random manner. As the active sites got saturated, the rate of adsorption gradually decreased till equilibrium was attained. It was observed that maximum percentage removal of 90.7% was obtained when contact time was 65 min.

3.5. Effect of mercury ion concentration

The effect of initial concentration of Hg(II) ion in the range of 5 to 30 mg L^{-1} was investigated using the optimum time (65 min), the amount of adsorbent (0.8 g) and pH 5. It was found that by increasing the initial concentration of mercury ions, amount adsorbed decreased as more effective adsorption sites are available for adsorption of mercury ions at lower concentration. With the increase in the amount of mercury ions, the number of active sites available for adsorption decreases. Hence, it is observed that the adsorption depends upon the initial concentration of Hg(II). At higher concentration of Hg(II), more active sites get covered and Hg(II) ions need to compete more for the free

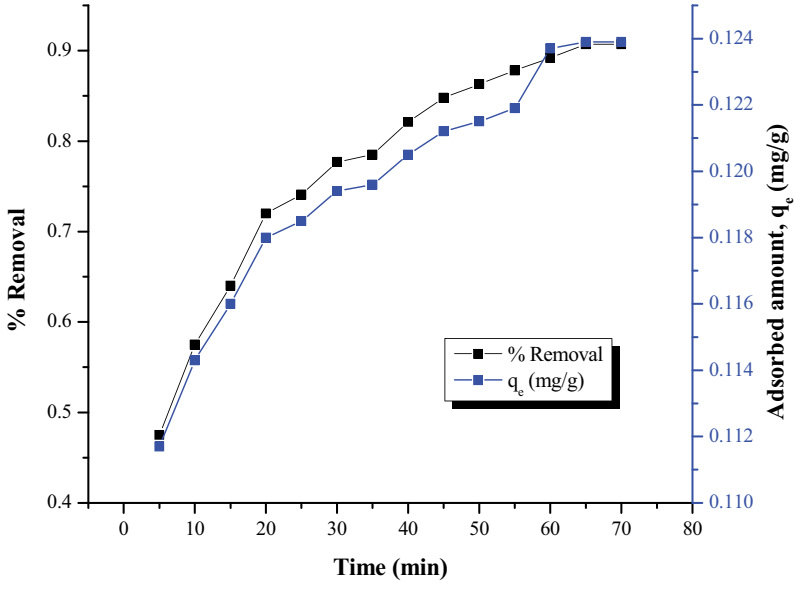

Figure 9. Effect of contact time on % removal and adsorbed amount of Hg(II). [Hg(II) = 10 mg L^{-1}, Adsorbent dose = 0.8 g, Temperature = 30°C and pH = 5].

sites available on the surface of the adsorbent. The effect of initial Hg(II) concentration on % removal of mercury is shown in Figure 10. It is evident that with increase in Hg(II) concentration there is a very slight increase in adsorption, especially at lower concentration region implying affinity performance [55].

3.6. Adsorption isotherms

Various adsorption isotherm models were used to determine the correlation between adsorbate and adsorbent under optimised condition. The equilibrium data obtained were fitted to different models, i.e. Freundlich [56], Langmuir [57], and Temkin isotherm [58]. The adsorption capacity of GFMNPECABs for removal of Hg(II) was also determined.

In the Langmuir's model, adsorption is monolayer in nature and is applicable under the conditions of low pressure. The Langmuir isotherm model is represented by Equation (4) as follows:

$$\frac{1}{q_e} = \frac{1}{q_m} + \frac{1}{K_m . q_e} . \frac{1}{C_e} \tag{4}$$

where K_m is the Langmuir adsorption constant (L mg^{-1}) and q_m is the maximum adsorption capacity of the adsorbent (mg g^{-1}). C_e and q_e are the equilibrium concentration of Hg(II) ion and its equilibrium adsorption capacities (mg L^{-1}). A plot $1/q_e$ versus $1/C_e$ is depicted in Figure 11(a).

The Langmuir isotherm model was explained using a dimensionless constant separation factor or equilibrium parameter R_L, which was calculated using Equation (5)

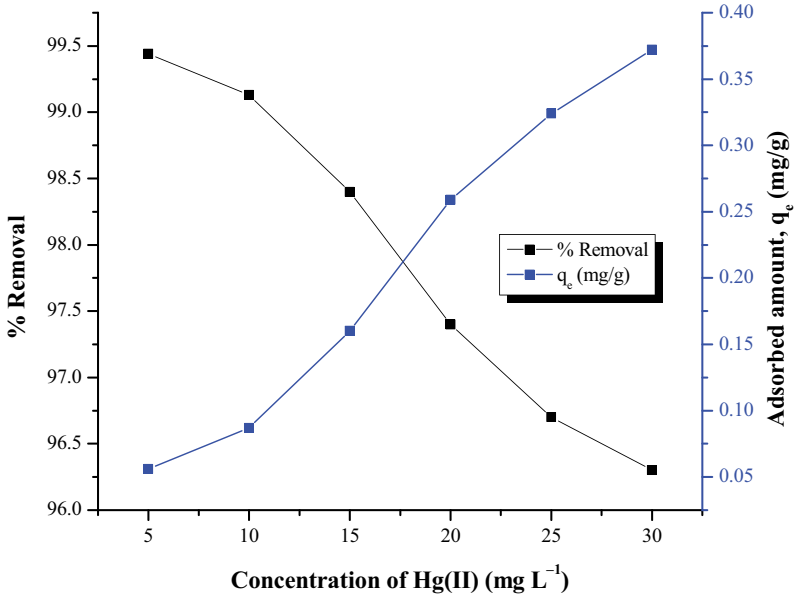

Figure 10. Effect of initial concentration of Hg(II) on % removal and adsorbed amount. Adsorbent dose = 0.8 g, Time = 65 min, pH = 5 and Temperature = 30°C.

$$R_L = \frac{1}{1 - K_L C_0} \tag{5}$$

The value of R_L infers that the adsorption is irreversible ($R_L = 0$), favourable ($0 < R_L < 1$), linear ($R_L = 1$) or unfavourable ($R_L > 1$). The value of R_L was very much less than 1, thereby confirming that the adsorption of Hg(II) was a favourable process [59–61].

The Freundlich model was applicable for adsorption on heterogeneous surface. This model describes reversible adsorption without any restriction to the formation of monolayer. The Freundlich model is expressed as Equation (6),

$$\log q_e = \log K_F + \frac{1}{n} \log C_e \tag{6}$$

where K_F ((mg g^{-1}) (mg $L^{-1})^n$) and n are Freundlich constants representing the adsorption capacity and intensity of the system, respectively. C_e and q_e were the equilibrium concentration of Hg(II) ion and equilibrium adsorption capacity (mg g^{-1}) respectively. The value of K_F and 1/n are obtained from slope and intercept of linear plot of log q_e versus log C_e shown in Figure 11(b).

Temkin isotherm model is based on the surface coverage wherein, adsorption energy decreases linearly with the amount of coverage. The Temkin isotherm has been expressed by Equation (7),

$$q_e = B_1 \ln K_T + B_1 \ln C_e \tag{7}$$

where $B_1 = RT/b$, b is the Temkin constant (J mol^{-1}), T is the absolute temperature (K), R is the gas constant (8.314 J mol^{-1} K), constant B_1 is related to the heat of adsorption (J mol^{-1}), K_T is the equilibrium binding constant (L g^{-1}). The determination of K_T and B_1 can

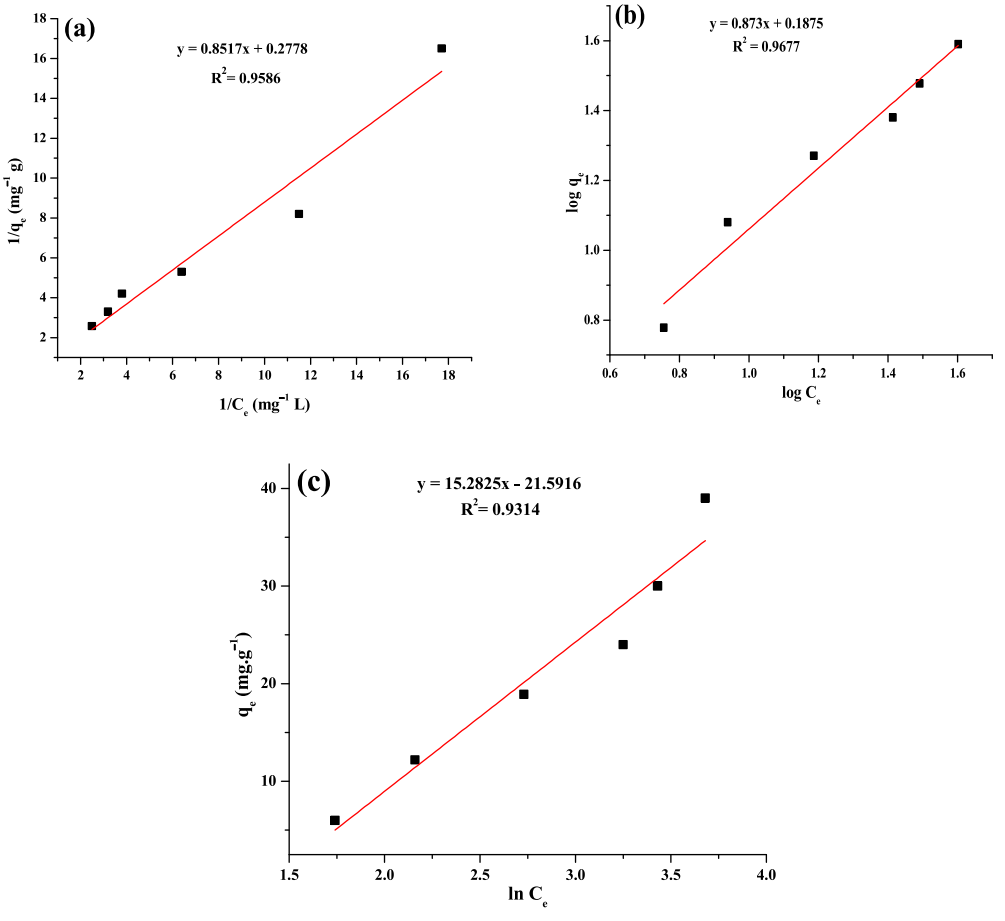

Figure 11. Adsorption isotherms (a) Langmuir, (b) Freundlich and, (c) Temkin for Hg(II) adsorption onto GFMNPECABs.

be made by plotting q_e versus ln C_e, shown in Figure 11(c). The experimental results are shown in Table 1. The data shows that it fits best with Freundlich isotherm model (R^2 = 0.9677) than Langmuir (R^2 = 0.9586) and Temkin model (R^2 = 0.9314) proving heterogeneity of surface. In literature, it was found that some pollutant-adsorbent isotherm results showed good fit with Freundlich isotherm models [62–65].

3.7. Mercury adsorption kinetics

To investigate the mercury adsorption kinetics, the pseudo-first-order model [65], pseudo-second-order model [66], Elovich kinetics model [67], and intra-particle diffusion model [68] were used. The effect of variation of contact time on adsorption on GFMNPECABs is depicted in Figure 12.

The pseudo-first order kinetics equation, pseudo-second order kinetics equation, Elovich kinetics model and intra-particle diffusion have been evaluated by the following Equations (8–11):

Table 1. Adsorption isotherm parameters for Hg(II) adsorption on GFMNPECABs.

Isotherm	Value of parameters			
Langmuir	q_{max} (mg g^{-1}) 3.59	K_L 3.0576	R^2 0.9586	R_L 0.0314
Freundlich	K_F (mg g^{-1}) (mg $L^{-1})^n$ 1.5399	n 1.1454	R^2 0.9677	
Temkin	B_1 15.2528	K_T (L mg^{-1}) 0.2434	R^2 0.9314	

$$\log(q_e - q_t) = \log q_e - \frac{k_1 t}{2.303} \tag{8}$$

where q_e and q_t are the amount of mercury adsorbed (mg g^{-1}) at equilibrium and at given time, t (min), respectively, and k_1 (min^{-1}) is the rate constant for pseudo-first-order equation. The plot log (q_e – q_t) versus t plot is shown in Figure 12(a).

$$\frac{t}{q_t} = \frac{t}{k_2 q_e^2} - \frac{1}{q_e} \tag{9}$$

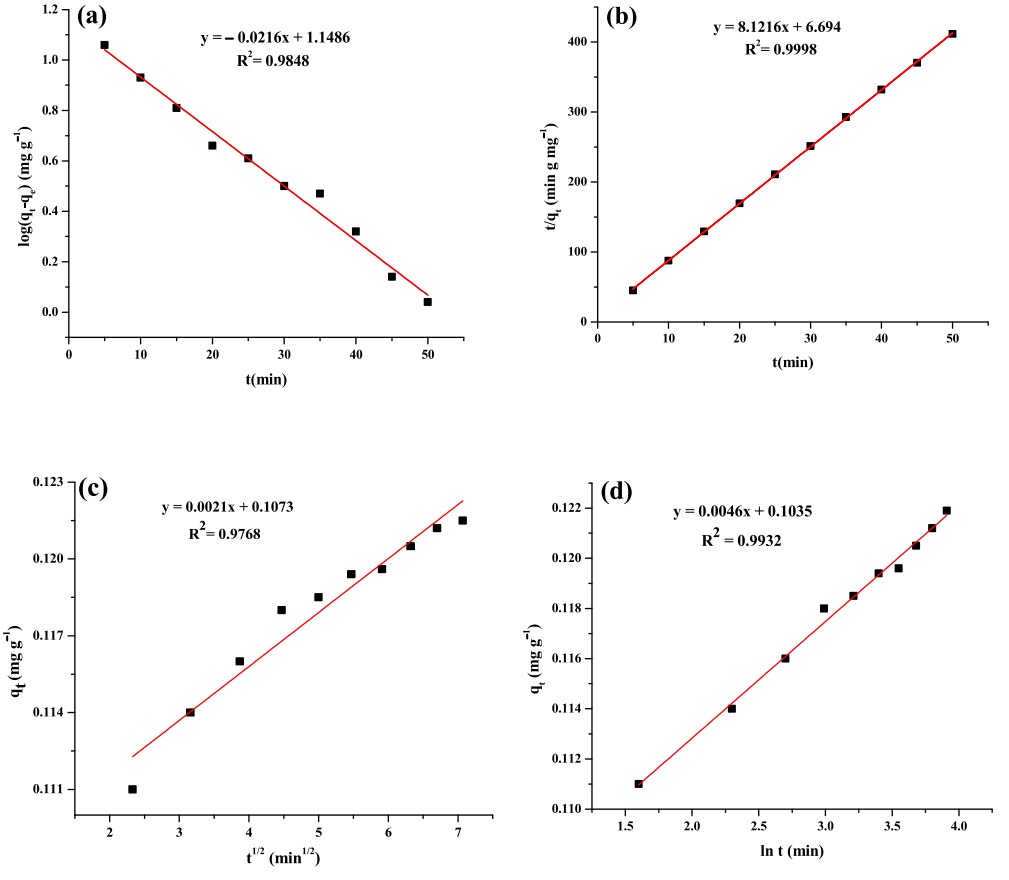

Figure 12. Plot of various kinetic models: pseudo-first order model (a), pseudo-second order models (b) intra-particle diffusion (c) and Elovich model (d).

where k_2 (g mg^{-1} min^{-1}) is rate constant for pseudo-second order and q_e and q_t are same as above. The plot t/q_t versus t is shown in Figure 12(b). The highest correlation was coefficient obtained for the pseudo-second order.

According to the intra-particle diffusion model based on the diffusion mechanism, proposed by Weber and Morris:

$$q_t = K_d t^{1/2} + C \tag{10}$$

where K_d is the diffusion rate constant in the pores (mg g^{-1} min$^{1/2}$) and C is the intercept (mg g^{-1}). The plot d_t versus $t^{1/2}$ is shown in Figure 12(c).

Elovich equation is used for the general application to chemisorption and this equation applies satisfactorily for chemisorption process, which implies formation of multilayer adsorption. The equation is expressed as below:

$$q_t = \alpha + \beta \ln t \tag{11}$$

where constant α (mg g^{-1} min^{-1}), β (g mg^{-1}) and q_t (mg g^{-1}) is the amount of mercury(II) adsorbed at time t (min). The values of β and α were obtained from the slope and intercept of the linear plot of q_t versus ln t as shown in Figure 12(d). The correlation coefficients (R^2) and other kinetics parameters are shown in Table 2 for the four models.

Result showed that the highest R^2 value corresponds to the pseudo-second-order model with R^2 equal to 0.9998. In literature, similar kinetic results were reported for the adsorption kinetic of various water pollutants by different carbon- and clay-based adsorbents [69–71].

3.8. Thermodynamic parameters

The thermodynamic parameters, such as Gibbs free energy (ΔG°, kJ mol^{-1}), enthalpy change (ΔH°, kJ mol^{-1}) and entropy change (ΔS°, J mol^{-1} K^{-1}) were determined using the equilibrium data at different temperatures by Gibbs equation and Van't Hoff equation as follows:

$$\Delta G^{\circ} = -RT \ln K_d \tag{12}$$

$$\ln K_d = \frac{\Delta S^{\circ}}{R} - \frac{\Delta H^{\circ}}{RT} \tag{13}$$

Table 2. Kinetic parameters for the adsorption of mercury onto GFMNPECABs.

Models	Kinetics Parameters		
Pseudo-First-Order	k_1 (min^{-1}) 0.048	q_e(mg g^{-1}) 0.0601	R^2 0.9848
Pseudo-Second-Order	k_2 (g mg^{-1} min^{-1}) 9.9009	q_e (mg g^{-1}) 0.1231	R^2 0.9998
Intra-particle Diffusion	k_d (mg g^{-1} min^{-1}) 0.0021	C (mg g^{-1}) 0.1073	R^2 0.9768
Elovich model	A (mg g^{-1} min^{-2}) 0.1035	β (g mg^{-1} min^{-1}) 0.0046	R^2 0.9932

where K_d is the equilibrium constant in Langmuir model (L/g), T is the absolute temperature (Kelvin, K), R is the universal gas constant (8.314 kJ mol^{-1} K). The values of ΔH^o and ΔS^o was determined from the slope and the intercept of the plot of ln K_d versus 1/T (Figure 13). Van't Hoff equation relates distribution coefficient with ΔH^o and ΔS^o at constant temperature. The ΔH^o and ΔS^o evaluated as 20.25 kJ mol^{-1} and 79.88 J mol^{-1} K^{-1}, respectively. The positive value of enthalpy and entropy indicates the endothermic and spontaneous nature of adsorption of Hg(II). Similar endothermic adsorption behaviour was reported for many adsorbent-pollutant systems in literature [72,73]. The value of ΔG was calculated to be – 3.77, – 5.12 and – 6.33 kJ mol^{-1} at 30°C, 40°C and 50°C, respectively, which indicates that the adsorption of Hg(II) on GFMNPECABs was thermodynamically feasible and spontaneous at all temperatures.

3.9. Desorption

Desorption experiments were achieved by using 0.05 M HCl solution as a desorption agent. For studying desorption of Hg(II) on GFMNPECABs, the optimised condition was as follows: initial concentration of Hg(II) ions 10 mg L^{-1}; amount of adsorbent 0.8 g; pH 5; temperature 30°C; contact time 65 min. The adsorbent was then placed in the desorption medium and stirred at a rate of 500 rpm for 140 min. The reusability of the adsorbent was found, after four cycles of adsorption–desorption (Figure 14). The results show that the desorption of GFMNPECBs sample was 97.53%, by the fourth cycle. The GFMNPECBs adsorbent was washed several times with deionised water and had a good adsorption-desorption performance and can be used without significant reduction in its adsorption capacity. The desorption (%) was calculated by

$$D\% = \frac{C_{des}}{C_0} \times 100 \tag{14}$$

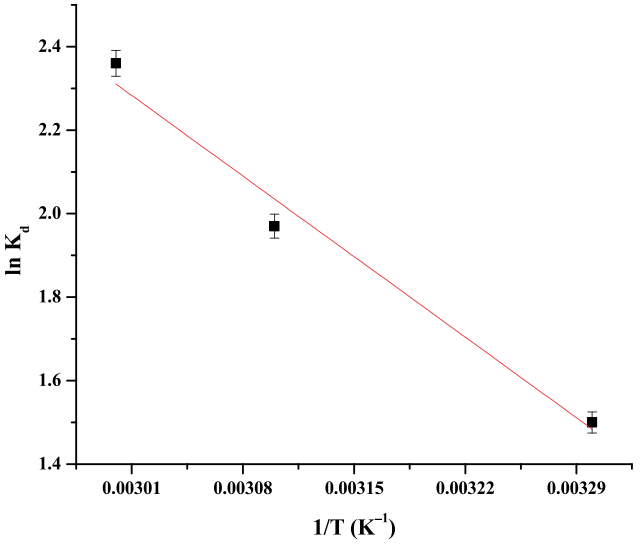

Figure 13. Van't Hoff's plot for adsorption of Hg (II) on GFMNPECABs.

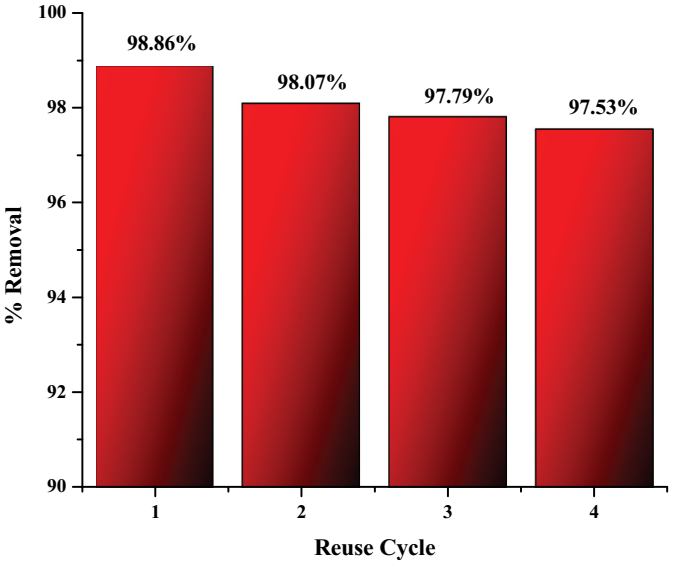

Figure 14. Relationship between reuse cycles and the % removal of Hg(II) ions by GFMNPECABs. [Hg(II) = 10 mg L^{-1}, temperature = 30°C, adsorbent dose = 0.8 g and pH = 5].

where C_{des} and C_o are the desorption equilibrium concentration (mg L^{-1}) and initial concentration (mg L^{-1}), respectively.

3.10. Adsorption mechanism

The FTIR spectra of GFMNPECABs (Figure 3) show shift of band position and intensity at 3567, 3395, 2927, 1604 and 1412 cm^{-1} after adsorption of Hg(II). These results indicate that the N–H, OH, C–H and COO^- groups are involved in the adsorption process. Figure 15 represents the mechanism for adsorption of Hg(II) ions by GFMNPECABs (a) and reaction used for study of adsorption (b). GFMNPECABs and other adsorbents have been reported to involve surface complexation by coordination and electrostatic attraction between non-protonated amine groups and metal ions [40,47,74]. In addition, the maximum adsorption was observed at pH 5 (above pH_{pzc} = 4.76), when the surface is negatively charged which may result in the surface complexation of non-protonated amine with mercury.

3.11. Comparison with other adsorption methods

The comparison of adsorption capacity of various adsorbents for Hg(II) are given in Table 3. It was found from the table that the GFMNPECABs had a good affinity for removal of mercury compared with other adsorbents.

4. Conclusion

The current study shows that GFMNPECABs is a promising, cost-effective and eco-friendly means for the removal of Hg(II) ions from water samples and the spectrophotometric

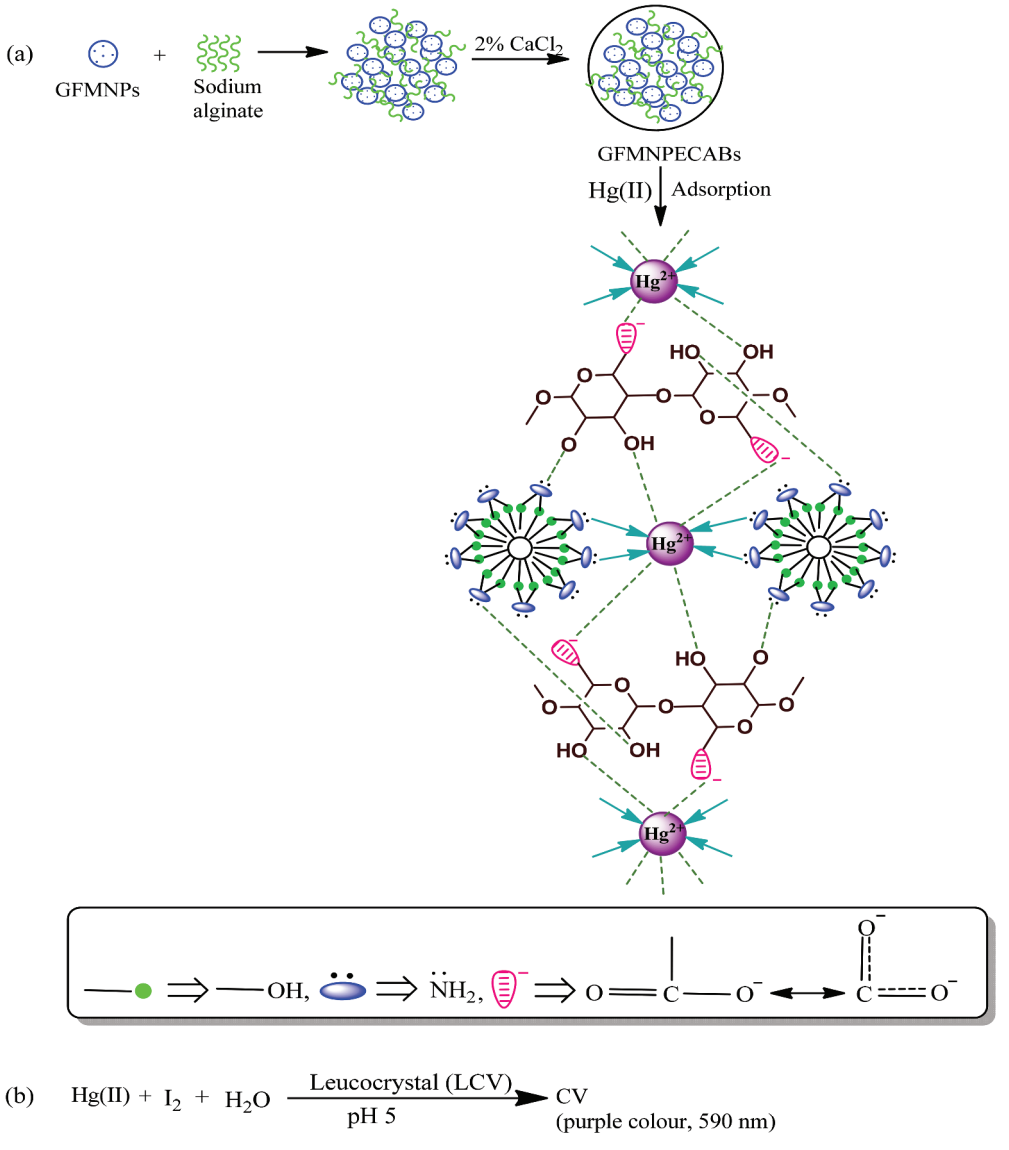

Figure 15. Schematic representation of mechanism for adsorption of Hg(II) ions by GFMNPECABs (a) and reaction used for study of adsorption (b).

method based on reaction of Hg(II) with iodine and LCV can be used for monitoring the adsorption of Hg(II). GFMNPECABs were quite effective for removal of Hg(II) ions from aqueous solution due to its microporous structure with high specific surface area. The adsorption isotherm followed Freundlich model with maximum adsorption capacity of 3.59 mg g^{-1} in 65 min at pH 5 and the kinetic data indicated that it follows pseudo-second -order model. The GFMNPECABs could be easily separated by external magnetic field and hence can be used as an effective and safe adsorbent for the removal of Hg(II) from waste water following the principles of green chemistry.

Table 3. Adsorption capacities of different adsorbents – a comparison.

Adsorbents	Adsorption Capacity (mg g^{-1})	References
Mercaptoethylamine/mercaptopropyltrimethoxysilane functionalised vermiculites	0.28	[75]
Bamboo (activated carbon precursor)	2.71	[76]
Dithizone-immobilised zeolite	2.60	[77]
Calixarene/Fe hybrid	0.43	[78]
Modified Fe oxide	0.59	[79]
Activated Carbon	0.86	[80]
Palm leaves	0.29	[81]
GFMNPECABs	3.59	Present study

Acknowledgments

One of the Authors(S L) acknowledge Pt. Ravishankar Shukla University for Research Scholarship (no. 3114/8/Fin./Sch.//2018), NIT Raipur for XRD studies, SAIF Cochin for FTIR, SEM analysis and MNIT Jaipur for BET analysis. The authors are thankful to the Department of Chemistry of the Govt. V.Y.T. PG Autonomous College, Durg, Chhattishgarh, India for providing the necessary lab facilities.

Disclosure statement

The authors declare that they have no conflict of interest.

Funding

This work was supported by the Pt. Ravishankar Shukla University Raipur from Pt. Ravishankar Research Fellowship Scheme, grant number V.R. No. 3114/8/Fin./Sch.//2018.

ORCID

Ajaya Kumar Singh http://orcid.org/0000-0001-8180-7292

References

[1] C. Arpa, A. Saglam, S. Bektas, S. Patir, O. Genc and A. Denizli, Adsorpt. Sci. Technol. **20** (3), 203 (2002).
[2] K. Pillay, E.M. Cukrowska and N.J. Coville, Microchem. J. **108**, 124 (2013).
[3] T. Dewangan, A. Tiwari and A.K. Bajpai, Taylor Francis **31**, 844 (2010).
[4] R. Bhatt and P. Padmaj, Carbohydr. Polym. **207**, 663 (2019).
[5] H. Sadegh, G.A.M. Ali, A.S.H. Makhlouf, K.F. Chong, N.S. Alharbi, S. Agarwal and V.K. Gupta, J. Mol. Liq. **258**, 345 (2018).
[6] G.P. Pandey, A.K. Singh, S. Prasad, L. Deshmukh, A. Asthana, S.B. Mathew and M. Yoshida, Microchem. J. **128**, 55 (2016).
[7] S. Mauchauffée and E. Meux, Chemosphere **69**, 763 (2007).
[8] A.G. El Samrani, B.S. Lartiges and F. Villiéras, Water Res. **42**, 951 (2008).
[9] J. Yoon, G. Amy, J. Chung, J. Sohn and Y. Yoon, Chemosphere **77**, 228 (2009).
[10] T. Phothitontimongkol, N. Siebers, N. Sukpirom and F. Unob, Appl. Clay Sci. **43** (3), 343 (2009).
[11] J. Gao, S.P. Sun, W.P. Zhu and T.S. Chung, Water Res. **63**, 252 (2014).
[12] T.S. Anirudhan, L. Divya and M. Ramachandran, J. Hazard. Mater. **157**, 620 (2008).
[13] C.M. Futalan, C.C. Kan and M.L. Dalida, Carbohydr. Polym. **83**, 528 (2011).

[14] A.A. Atia, Hydrometallurgy **80**, 13 (2005).
[15] V.K. Gupta, S.K. Srivastava and D. Mohan, Ind. Eng. Chem. Res. **36** (6), 2207 (1997).
[16] C. Liu, P. Wu, Y. Zhu and L. Tran, Chemosphere **144**, 1026 (2016).
[17] D.K. Mondal, B.K. Nandi and M.K. Purkait, J. Environ. Chem. Eng. **1**, 891 (2013).
[18] B. Qiu, H. Gu, X. Yan, J. Guo, Y. Wang, D. Sun, Q. Wang, M. Khan, X. Zhang and B. Weeks, J. Mater. Chem. **2**, 17454 (2014).
[19] H. Xu, J. Xie, Y. Ma, Z. Qu, S. Zhao, W. Chen, W. Huang and N. Yan, Fuel **140**, 803 (2015).
[20] B. Petrie, R. Barden and B. Kasprzyk-Hordern, Water Res. **72**, 3 (2015).
[21] L. Yu, Y. Ma, C.N. Ong, J. Xie and Y. Liu, RSC Adv **5**, 64983 (2015).
[22] Y. Liu, C.N. Ong and J. Xie, Nanotechnol. Rev. **5** (1), 1 (2016).
[23] M.R. Awual, M. Ismael and T. Yaita, Sensor. Actuat. B-Chem. **191**, 9 (2014).
[24] J. Tang, J. He, T. Liu and X. Xin, RSC Adv **7**, 33385 (2017).
[25] A. Asthana, R. Verma, A.K. Singh, M.A.B.H. Susan and R. Adhikari, Macromol. Symp. **366**, 42 (2016).
[26] R. Verma, A. Asthana, A.K. Singh, S. Prasad and A.B.H. Susan, Microchem. J. **130**, 168 (2017).
[27] L.H. Ai, H.Y. Huang, Z.L. Chen, X. Wei and J. Jiang, Chem. Eng. J. **156**, 243 (2010).
[28] G. Neeraj, S. Krishnan, P.S. Kumar, K.R. Shriaishvarya and V.V. Kumar, J. Mol. Liq. **214**, 335 (2016).
[29] L. Zhou, Z. Liu, J. Liu and Q. Huang, Desalination **258**, 41 (2010).
[30] M.M. Lakouraj, F. Hasanzadeh and E.N. Zare, Iran. Polym. J. **23**, 933 (2014).
[31] L. Chen, P. Wu, M. Chen, X. Lai, Z. Ahmed, N. Zhu, Z. Dang, Y. Bi and T. Liu, Appl. Clay Sci. **159**, 74 (2018).
[32] A.Z. Badruddoza, M.T. Rahman, S. Ghosh, M.Z. Hossain, J.Z. Shi, K. Hidajat and M.S. Uddin, Carbohydr. Polym. **95** (1), 449 (2013).
[33] X.B. Zhang, Y. Wang and S.T. Yang, Carbohydr. Polym. **114**, 521 (2014).
[34] A. Idris, N.S.M. Ismail, N. Hassan, E. Misran and A.F. Ngomsik, J. Ind. Eng. Chem. **18**, 1582 (2012).
[35] A.N. Bezbaruah, S. Krajangpan, B.J. Chisholm, E. Khan and J.J. Bermudez, J. Hazard. Mater. **166**, 1339 (2009).
[36] M.M. Lakouraj, F. Mojerlou and E.N. Zare, Carbohydr. Polym. **106**, 34 (2014).
[37] R. Mahalakshmi, L. Ravikumar and K. Rathina, RASAYAN J. Chem. **10** (1), 286 (2017).
[38] M. Yadav, K. Rani, M.K. Chauhan, A. Panwar and N. Sandal, J. Appl. Phycol. **32**, 1253 (2020).
[39] R. Verma, A. Asthana, A.K. Singh and M.A.B.H. Susan, J. Environ. Chem. Eng. **4**, 1985 (2016).
[40] M. Naushad, T. Ahamad, Z.A. AlOthman and A.H. Al-Muhtaseb, J. Mol. Liq. **279**, 1 (2019).
[41] S. Lilhare, S.B. Mathew, A.K. Singh and S.A.C. Carabineiro, Anal. Chem. **10**, 654 (2020).
[42] J. Wang, K. Pan, Q. He and B. Cao, J. Hazard. Mater. **244**, 121 (2013).
[43] M. Singh, H.S. Dosanjh and H. Singh, J. Water Process Eng. **11**, 152 (2016).
[44] O. Duman, S. Tunc, T.G. Polat and B.K. Bozoglan, Carbohydr. Polym. **147**, 79 (2016).
[45] O. Duman, S. Tunç, B.K. Bozoğlan and T.G. Polat, J. Alloys Compd. **687**, 370 (2016).
[46] O. Duman, C. Özcan, T.G. Polat and S. Tunç, Environ. Pollut. **244**, 723 (2019).
[47] Z. Ahmed, P. Wu, L. Jiang, J. Liu, Q. Ye, Q. Yang and N. Zhu, Colloid. Surface. A **604**, 125285 (2020).
[48] P.A. Cormack and A.Z. Elorza, J. Chromatogr. B. **804**, 173 (2004).
[49] N.C. Feitoza, T.D. Goncalves, J.J. Mesquit, J.S. Menegucci, M.M.S. Santos, J.A. Chaker, R. B. Cunha, A.M.M. Medeiros, J.C. Rubim and M.H. Sousa, J. Hazard. Mater. **264**, 153 (2014).
[50] Q. Ye, J. Wu, P. Wu, J. Wang, W. Niu, S. Yang, M. Chen, S. Rehman and N. Zhu, Water Res. **185**, 116246 (2020).
[51] S. Liu, P. Wu, M. Chen, L. Yu, C. Kang, N. Zhu and Z. Dang, Environ. Pollut. **228**, 277 (2017).
[52] K.S.W. Sing, D.H. Everett, R.A.W. Haul, L. Moscou, R.A. Pierotti, J. Rouquerol and T. Siemieniewska, Pure Appl. Chem. **57** (4), 603 (1985).
[53] R. Verma, A. Asthana, A.K. Singh and S. Prasad, RSC Adv **7**, 51079 (2017).
[54] M. Kumar, H.S. Dosanjh and H. Singh, Fibers Polym. **20** (4), 739 (2019).
[55] M.A.A. Ganzagh, M. Yousefpour and Z. Taherian, J. Chem. Biol. **9**, 127 (2016).
[56] H. Freundlich, Z. Phys. Chem. **57**, 385 (1906).
[57] I. Langmuir, J. Am. Chem. Soc. **38**, 2221 (1916).

[58] M.I. Temkin and V. Pyzhev, Acta. Phys-Chim. **12**, 327 (1940).
[59] A. Naghizadeh, F. Ghasemi, E. Derakhshani and H. Shahabi, Desalin. Water Treat. **80**, 247 (2017).
[60] A. Naghizadeh and K. Gholami, J. Water Health **15**, 555 (2017).
[61] M. Kamranifar and A. Naghizadeh, Iran. J. Chem. Chem. Eng. **36**, 127 (2017).
[62] O. Duman and E. Ayranci, Sep. Sci. Technol. **41**, 3673 (2006).
[63] O. Duman and E. Ayranci, J. Hazard. Mater. B **120**, 173 (2005).
[64] C.K. Ahn, D. Park, S.H. Woo and J.M. Park, J. Hazard. Mater. **164**, 1130 (2009).
[65] S. Lagergren, Sven. Vetenskapsakad. Handlingar **24**, 1 (1898).
[66] G. Bayramoglu, B. Altintas, M.Y. Arica, Chem. Eng. J. **152**, 339 (2009).
[67] S.H. Chien and W.R. Layton, Soil Sci. Soc. Am. J. **44**, 265 (1980).
[68] F.C. Wu, R.L. Tseng and R.S. Juang, Chem. Eng. J. **153**, 1 (2009).
[69] E. Ayranci and O. Duman, Chem. Eng. J. **156**, 70 (2010).
[70] O. Duman, S. Tunç and T.G. Polat, Appl. Clay Sci. **109**, 22 (2015).
[71] O. Duman and E. Ayranci, J. Hazard. Mater. **174**, 359 (2010).
[72] O. Duman, S. Tunç and T.G. Polat, Micropor. Mesopor. Mat. **210**, 176 (2015).
[73] O. Duman, T.G. Polat, C.Ö. Diker and S. Tunç, Int. J. Biol. Macromol. **160**, 823 (2020).
[74] M. Chen, S. Li, L. Liping, L. Jiang, Z. Ahmed, Z. Dang and P. Wu, J. Hazard. Mater. **401**, 123447 (2021).
[75] L. Tran, P. Wu, Y. Zhu, L. Yang and N. Zhu, J. Colloid Interface Sci. **445**, 348 (2015).
[76] Z. Tan, J. Qiu, H. Zeng, H. Liu and J. Xiang, Fuel **90**, 1471 (2011).
[77] M. Mudasir, K. Karelius, N.H. Aprilita and E.T. Wahyuni, J. Environ. Chem. Eng. **4**, 1839 (2016).
[78] A. Bhattia, M. Oguza and M. Yilmaz, Appl. Surf. Sci. **434**, 1217 (2018).
[79] H. Parham, B. Zargar and R. Shiralipour, J. Hazard. Mater. **205**, 94 (2012).
[80] S.H. Park, S.O. Hwang, T.S. Kim, A. Cho, S.J. Kwon, K.T. Kim, H.D. Park and J.H. Lee, Appl. Surf. Sci. **443**, 458 (2018).
[81] M. Mohammadi, K. Shamsi, A. Dargahi and P. Sekhavati, J. Environ. Health Res. **5**, 101 (2017).